Bulgarian Chemical Communications, Volume 52, Special Issue E (pp. 21 - 27) 2020

Electrophoretic deposition of boehmite particles to improve the anti-corrosion behavior of anodized aluminum alloy 2024-T3

Florent Caubert[1], Pierre-Louis Taberna[1], Laurent Arurault[1*], Benoît Fori[2]

[1]*CIRIMAT, Université de Toulouse, CNRS, UT3 Paul Sabatier, Bât. CIRIMAT, 118 route de Narbonne, 31062 Toulouse cedex 9, France*

[2] *Mécaprotec Industries, 34 Boulevard Joffrery, 31605 Muret Cedex, France*

Received December 11, 2019; Accepted January 27, 2020

The purpose of this study was to prepare and evaluate a new two-step sealing process for a porous and tortuous anodic film, prepared on aluminum alloy (AA) 2024-T3, to ensure anti-corrosion properties. This process involves a cathodic electrophoretic deposition of boehmite particles, followed by a hydrothermal post-treatment. This two-step sealing was evaluated through three industrial tests (dye-spot, continuity and salt spray) and the low frequency resistance. Such sealing of the anodic film on AA 2024-T3 showed promising anti-corrosion behavior, suggesting a real potential interest of this innovative process for future industrial applications.

Keywords: Aluminum, porous anodic film, boehmite particles, electrophoretic deposition, hydrothermal post-treatment, sealing

INTRODUCTION

Due to their good mechanical properties and low density, aluminum alloys (AA), are intensively used in the aircraft industry [1,2], as with AA 2XXX (Al-Cu) or 7XXX (Al-Zn). However, Al-Cu alloys, for instance AA 2024, show a low corrosion resistance [3,4]. They therefore require an additional corrosion protection, usually obtained by (electro) chemical processes (i.e. typically anodizing and sealing), usually involving chemical solutions including hexavalent chromium-based compounds. Such compounds are known to be classified as being both highly toxic and carcinogenic and their use is limited by recently adopted European standards (REACH). So, to protect AA 2024 for instance, new alternatives have been studied and developed, such as new anti-corrosion coatings prepared via the sol-gel route [5], with corrosion inhibitors [6-10], as well as new green sealing of anodic films [11,12]. Electrophoretic deposition (EPD) of nanoparticles, from organic or aqueous media, could provide an interesting alternative since it is simple and cheap. In this process, particles migrate under the influence of an electric field and are deposited onto an electrode [13,14]. Organic media are usually used [15,16] due to their wide voltage range of electrochemical stability. For instance, Fori et al. [17,18] successfully filled a porous anodic film prepared on AA 1050 using SiO_2 nanoparticles dispersed in an isopropyl alcohol solution. But, for environmental reasons, the aqueous medium appears to offer a good alternative to avoid pollution. Despite a limited cell voltage due to water electrolysis, some previous studies [19-21] showed a significant incorporation of nanoparticles (SiO_2 and PTFE and AlOOH respectively) inside porous anodic films prepared on aluminum substrates. However, these results were obtained on pure aluminum substrates (99.99 % and 99.5 %) with anodic films showing straight pores, contrary to the tortuous porosity obtained when AA 2024 is anodized. Moreover, in previous studies [19-21], phosphoric acid-based electrolytes are used to perform anodizing to obtain the largest main pore diameter. However, the usual hydrothermal sealing of such anodic films prepared in phosphoric acid-based electrolyte is problematic [22] as compared with other types of anodic films.

There are now two main challenges:

- the first is to deposit nanoparticles on, and ideally in, the tortuous anodic film prepared on AA 2024 substrate,
- the second is to study a new process to seal the anodic film prepared in phosphoric acid-based electrolyte.

The present work aimed to develop a two-step sealing process for a tortuous anodic film prepared by anodizing of AA 2024-T3 in a phosphoric acid electrolyte. This sealing is implemented by direct electrophoretic deposition of boehmite nanoparticles dispersed in an aqueous solution on/into a tortuous anodic film, followed by a hydrothermal treatment. The resulting coatings are then characterized by FEG-SEM observations, and

* To whom all correspondence should be sent.
E-mail: arurault@chimie.ups-tlse.fr

evaluated through the low frequency resistance (50 mHz) – a good approximation of the polarisation resistance –, as well as using three standard industrial tests, i.e. salt spray, loss of absorptive power and continuity.

EXPERIMENTAL

Preparation

An aluminum alloy 2024-T3 substrate (compound of 4.5 % Cu, 1.5 % Mg, 0.6 % Mn, 0.2 % Fe, 0.08 % Zn, 0.06 % Si, 0.01 % Cr and 0.03 % Ti) was prepared following a three-step procedure (degreasing, etching and acid neutralization). Firstly, the aluminum sheet (20 x 20 x 1 mm or 80 x 1250 x 1 mm for industrial tests) was degreased using ethanol. The sample was then cleaned firstly in an alkaline aqueous solution (sodium triphosphate and borax) for 20 min at 60 °C (reaction 1).

$$Al_2O_3 + 2OH^- \rightarrow 2AlO_2^- + H_2O \quad (1)$$

Secondly, sample was then immersed in a sulfo-nitro-ferric acidic solution for 5 min at room temperature (reaction 2).

$$Al_2O_3 + 6H^+ \rightarrow 2Al^{3+} + 3H_2O \quad (2)$$

After being rinsed in deionized water (10^6 Ω.cm), the aluminum sheet was used as an anode and a lead plate (50 x 40 x 2 mm) as a cathode. The specimen was anodized at constant voltage (70 V for 60 min) in a phosphoric bath (40 $g.L^{-1}$, i.e. 0.48 $mol.L^{-1}$) at 25 °C (reactions 3 and 4). Finally, the obtained anodic film was fully rinsed in deionized water.

$$Al \rightarrow Al^{3+} + 3e^- \quad (3)$$

$$2Al^{3+} + 3O^{2-} \rightarrow Al_2O_3 \quad (4)$$

The first step of the sealing process involved a constant cathodic electrophoretic deposition of boehmite particles dispersed in an aqueous solution. A colloid suspension of boehmite nanoparticles in aqueous media was initially synthesized. This suspension was prepared by hydrolysis of an aluminum alkoxide following the Yoldas process [23] (reaction 5).

$$Al[OCH(CH_3)C_2H_5]_3 + H_2O \rightarrow AlOOH + 3C_4H_9OH \quad (5)$$

An excess of deionized water ($H_2O/Al = 100$) at 85 °C was then immediately added to 25.3 g of aluminum tri-sec-butoxide ($Al(OC_4H_9)_3$) while stirring for 15 min. The white sol obtained was peptized by adding 0.2 mol of nitric acid (HNO_3) per mole of alkoxide to improve particle dispersion. The mixture was then continuously stirred at 85°C for 24 h. The final concentration was around 0.5 $mol.L^{-1}$.

Electrophoretic impregnation of particles was then performed (10 V, 15 min) with the anodized aluminum substrate as the cathode, while a lead foil, located at about 2.5 cm from the cathode, was used as the anode. After being air dried for about 30min, a hydrothermal post-treatment (deionized water at 98 °C, 2 h) was performed as the second sealing step.

Characterizations and industrial tests

Surface and cross-sectional views of the coatings were performed using a Field Emission Gun Scanning Electron Microscope (FEG-SEM JEOL JSM 6700F).

The Stokes diameter of the nanoparticles and zeta potential of the particles were measured by Dynamic Light Scattering using a ZS90 Malvern nanosizer with zetasizer software.

The low frequency resistance (R_{LF}) of the samples was monitored for 240 h in a solution of NaCl (0.05 $mol.L^{-1}$) and Na_2SO_4 (0.5 $mol.L^{-1}$) at room temperature. A low concentration of chloride was chosen to limit the rapid corrosion attack, while sodium sulphate was chosen as a supporting electrolyte. A three-electrode electrochemical cell was used, with a platinum foil as a counter-electrode and a saturated calomel electrode as the reference electrode. The low frequency resistance was measured using an SP-150 BioLogic Science Instrument. It corresponds to the real part of the impedance measured at 50 mHz at open current potential; a RMS voltage amplitude of ± 50 mV_{eff} was applied.

Loss of absorptive power of the anodic films was evaluated by a dye-spot test according to ISO 2143 standard, while their continuity was evaluated with an acidic copper solution according to NF A 91410 standard. Additionally, salt spray tests were conducted for 24 h, according to EN ISO 2143 standard.

RESULTS AND DISCUSSION

After anodizing

Characteristics of the bare anodic film

FEG-SEM views (Figure 1) show that the bare porous anodic film (i.e. before electrophoretic deposition) typically has a thickness of 1.2 ± 0.3 μm. Although this thickness is low, the continuity test is compliant (Table 1) and so attests that the resulting anodic film is homogeneous and evenly covers the whole metal substrate.

Table 1. Results of both industrial continuity and dye-spot tests

Steps of the process	Dye-spot test	Continuity test
Anodizing	Grade 2	Conform
Anodizing + hydrothermal post-treatment	Grade 2	Conform
Anodizing + constant EPD + hydrothermal post-treatment	Grade 0	Conform

FEG-SEM views (Figure 1) additionally show that the porosity is extremely tortuous, much more so than the porosity obtained using purer 1050 aluminum alloy, in agreement with previous studies [24,25]. Despite the real difficulty in distinguishing the pores, their average diameter was estimated to be in the range of 30-50 nm. Unsurprisingly in this case, Grade 2 is obtained with a dye-spot test (Table 1), meaning that ink is impregnated into pores of the anodic film, indicating that the pores are not closed.

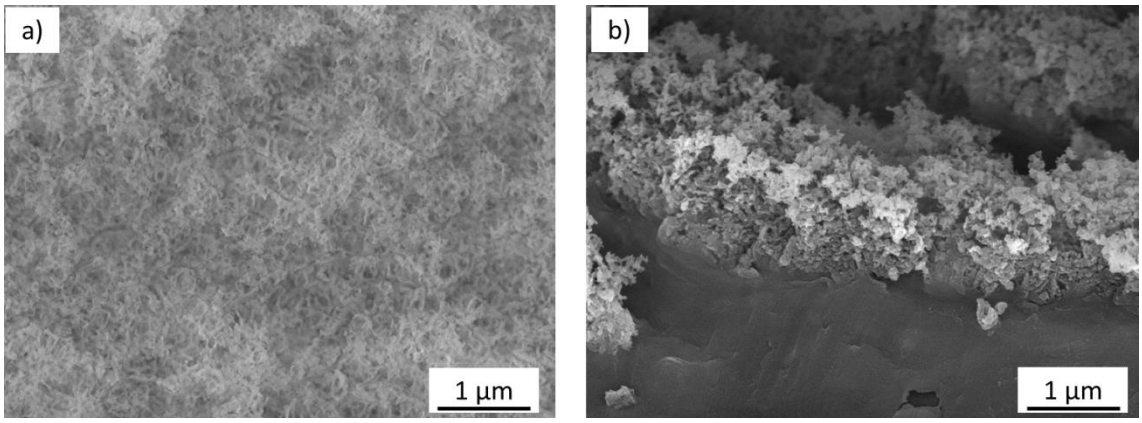

Fig. 1. FEG-SEM a) surface view and b) cross-sectional view of the bare porous anodic film, prepared (70V, 60 min, [H_3PO_4]=40 g.L^{-1}, 25°C) on AA 2024-T3

Corrosion behavior of the bare anodic film

Evaluation of the low frequency resistance was then performed in a solution including NaCl (0.05 mol.L^{-1}) and Na_2SO_4 (0.5 mol.L^{-1}), as a function of the immersion time (Figure 2). In comparison with the raw substrate, the anodized substrate shows a high low frequency resistance (about 1x10^5 Ω.cm^2) at the beginning of immersion (t = 0 h), proving the positive intake of the anodic film against corrosion. However, its resistance decreases and reaches a minimum (at about 1x10^3 Ω.cm^2) after 100 h of immersion (i.e. more than four days), meaning that the chloride corrosive ions penetrate through the barrier layer. This result is explained mainly by the opened pores and the thinness (1.2 ± 0.3 µm) of the bare anodic film, especially its barrier layer (lower than 100 nm). After 100 h, the bare anodic film shows the same behavior as the substrate, corrosion being generalized and the anodic film failing to further protect the AA substrate.

After the two-step sealing process
Characteristics of the sealed film

Diffusion Light Scattering analysis showed an average hydrodynamic diameter for the boehmite particles equal to 35±15 nm, while from zeta potential measurement it came out at +2.7x10^{-4} $cm^2.V^{-1}.s^{-1}$ as particle electrophoretic mobility. This positive value shows that it is possible to perform a cathodic electrophoretic deposition (here at 10 V), thus avoiding any further oxidation of the metal substrate, i.e. electrodissolution or over-oxidation of the aluminum [26]

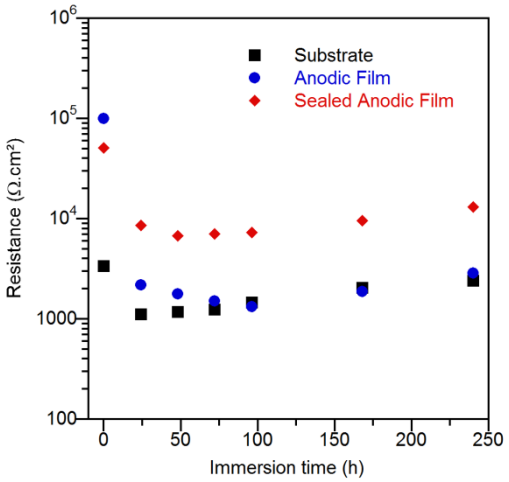

Fig. 2. Low frequency resistance values as a function of the immersion time

FEG-SEM views (Figure 3) show that electrophoresis alone induced a mainly top-surface deposit, although some of the smallest particles (about 20 nm) could be incorporated into the pores (30-50 nm).

The influence of the second sealing step, i.e. hydrothermal post-treatment (after the EPD), was then studied. FEG-SEM views (Figure 4) show complete sealing of the anodic film, both inside and on the top of the anodic film. On its top surface (Figure 4b), a typical "sand rose" structure is observed, attesting to the aluminum hydroxide formation. The continuity test gave a correct result (Table 1), meaning that the film is homogeneous and crack-free. In addition, after hydrothermal post-treatment, Grade 0 is obtained using the dye-spot test, since no color persists at the surface after removal of the dye-spot.

This result unambiguously proves that the pores are globally closed, in agreement with the FEG-SEM views (Figure 4).

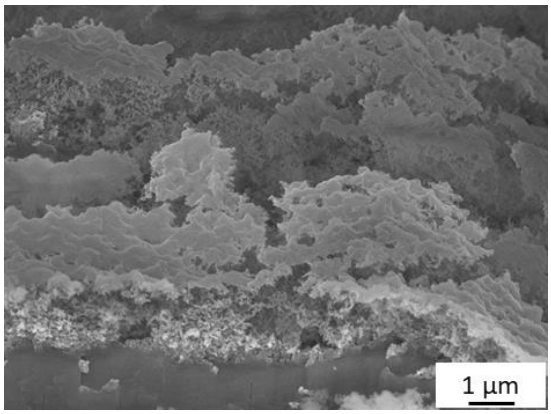

Fig. 3. FEG-SEM cross-sectional view of the anodic film after constant EPD (10 V, 15 min)

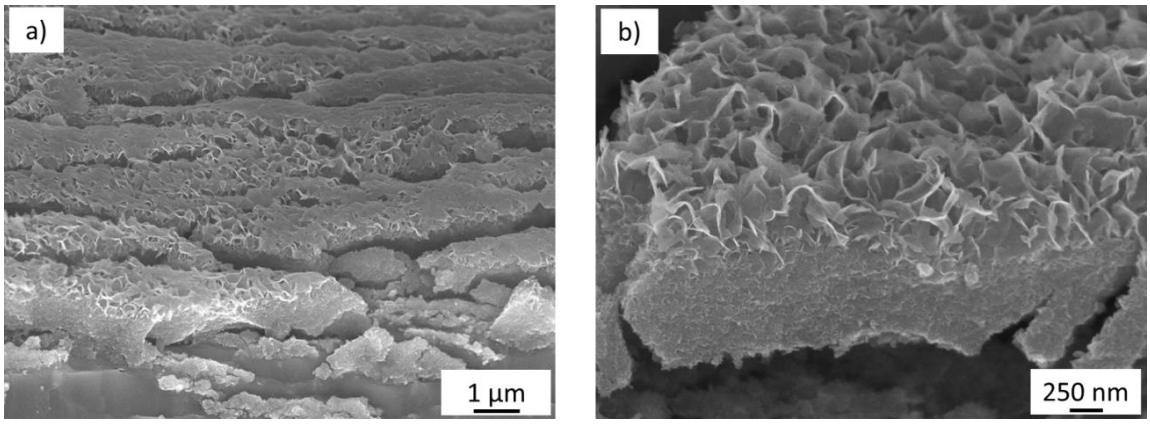

Fig. 4. FEG-SEM cross-sectional views of the anodic film after constant EPD (10 V, 15 min) followed by the hydrothermal post-treatment (deionized water at 98 °C, 2 h)

This result, i.e. complete sealing of the porosity, tends to prove either modification of particles on and inside the anodic film, or the film's transformation under hydrothermal conditions. To test these hypotheses, the same hydrothermal treatment was performed directly on the bare anodic film, i.e. without electrophoretic deposition. FEG-SEM views (Figure 5) show that no change can be observed in comparison with the bare anodic film (Figure 1). Moreover, while the industrial continuity test remains compliant (Table 1), grade 2 is again obtained with the industrial dye-spot test, proving that the pores are still partially unclosed following the hydrothermal treatment alone. Thus, in these conditions the usual hydrothermal sealing fails to occur, meaning there is no fast hydration of the pore walls of the bare anodic film. These results confirm the difficulty, for an anodic film prepared in phosphoric acid electrolyte, of sealing under the usual hydrothermal conditions [27]. This behavior can be explained by the incorporation of phosphate ions into the anodic film during its formation, largely inhibiting the latter's hydration [22]. The phosphate ions are indeed incorporated into the film in the form of aluminum phosphate $AlPO_4$ [28,29], which is thermo-dynamically stable. Davis et al. [22] showed that the $AlPO_4$ top-layer slowly dissolves and that this dissolution is the rate-limiting step inducing greater hydration resistance and thus impeding rapid sealing of the anodic film pores. In all events, our results clearly show that the electrophoretic deposition of boehmite particles allows the complete sealing of the tortuous anodic film prepared in phosphoric acid electrolyte on AA 2024-T3 to be achieved. In this case, the electrophoretic process followed by a hydrothermal post-treatment could jointly accelerate aluminum phosphate dissolution, thus allowing the hydration of the pore walls from alumina (Al_2O_3) to boehmite (AlOOH) (at T > 80°C) and subsequent interaction with the electrodeposited boehmite particles.

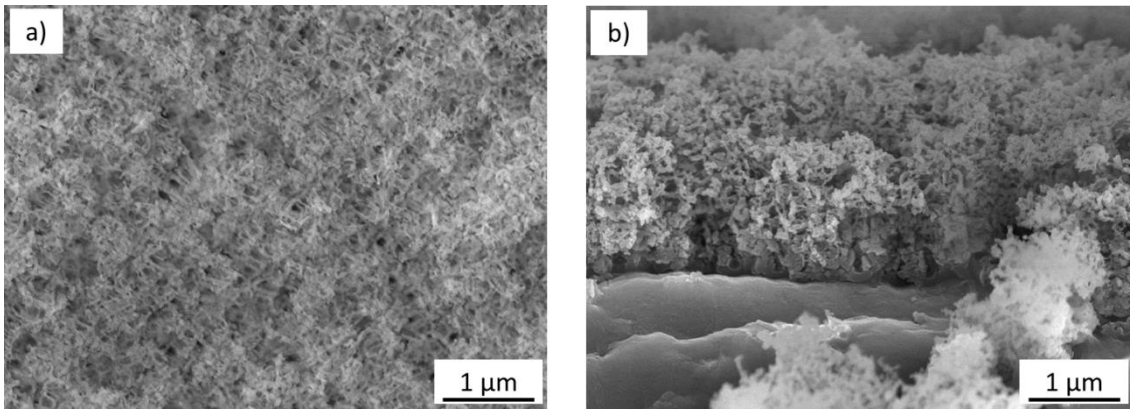

Fig. 5. FEG-SEM a) surface view and b) cross-sectional view of the anodic film after the hydrothermal post-treatment (deionized water at 98°C, 2h)

Corrosion behavior of the sealed film

Sealed film shows a similar behavior (Figure 2) compared with the bare anodized substrate for the first 50 h of immersion, with the low frequency resistance initially being high (about $5x10^4$ $\Omega.cm^2$). The R_{LF} of the sealed film then decreases but remains higher (about $8x10^3$ $\Omega.cm^2$) compared with the value obtained with the bare anodic film. After 50 h and up to 240 h (i.e. 10 days), the low frequency resistance of the sealed film slowly increases, significantly remaining higher than the value corresponding to the bare anodic film. Thus, this two-step sealing process clearly provides a barrier slowing down the penetration of corrosive species across the anodic film, and significantly improving the anti-corrosion behavior of AA 2024-T3.

Anodized samples with and without electrophoretic impregnation, but each time followed by the same hydrothermal post-treatment, were then characterized using the salt spray test. Figure 6 shows photographs of samples after a salt spray exposure for 24 h. Anodized samples without impregnation and with hydrothermal post-treatment are completely corroded (Figure 6a), whereas anodized samples with impregnation and identical post-treatment show only a few pits (Figure 6b). These results clearly indicate that this two-step sealing process, including electrophoretic deposit before hydrothermal post-treatment, successfully improves corrosion resistance of anodized AA 2024-T3. However, corrosion performances still fail to meet industrial requirements from the duration point of view; although the process can advantageously replace currently used techniques, it still needs to be optimized.

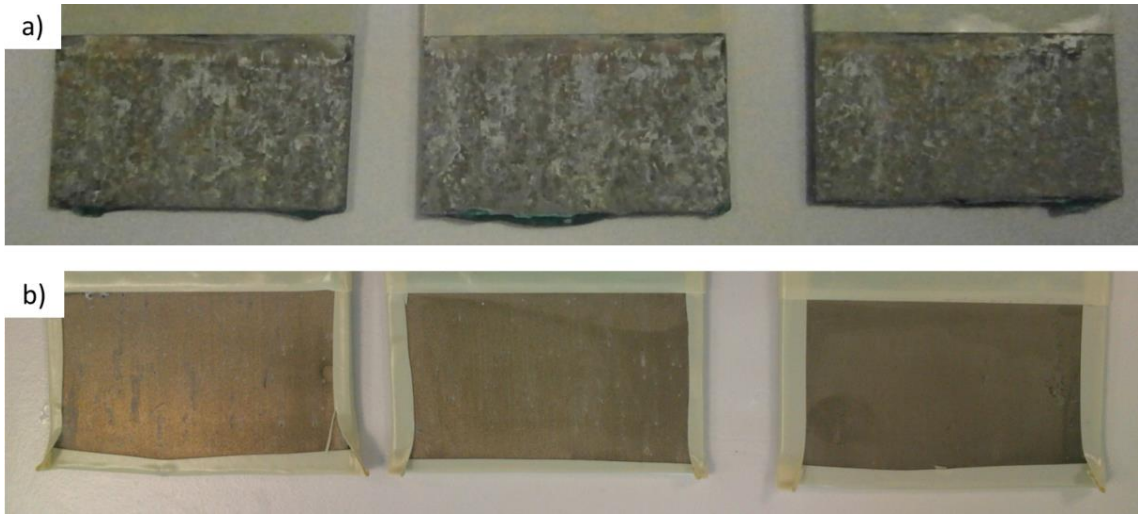

Fig. 6. After 24 h of salt-spray test, photographs of a) the anodic film after the hydrothermal post-treatment (deionized water at 98 °C, 2 h), and of b) the anodic film after constant EPD (10 V, 15 min) followed by the hydrothermal post-treatment

CONCLUSIONS

Anodizing of AA 2024-T3 was performed in phosphoric acid solution, with the resulting bare anodic film showing a low thickness (1.2 ± 0.3 µm) and tortuous porosity. Despite these conditions, the bare anodic film, and especially its barrier layer, provides a first level of protection against corrosion. To boost this protection, a constant cathodic electrophoretic deposition of boehmite particles ($Ø_{particles}$ = 35±15 nm) dispersed in an aqueous media was conducted, with the resulting deposit being mainly located on the surface. The process was completed by a second step, i.e. an additional hydrothermal post-treatment allowing the anodic film to be completely sealed. Finally, low frequency resistance characterization and three additional tests highlight positive and promising performances against corrosion thanks to the two-step sealing process. The results still fail to meet industrial expectations but the future use of pulsed electrophoresis could possibly offer a promising optimization technique to improve incorporation of the boehmite particles within the tortuous anodic film and thus enhance its anti-corrosion protective behavior.

Acknowledgements: *The present work was carried out as a part of the ECOREV project. The Regional Council of Midi-Pyrénées and Mecaprotec Industries are gratefully acknowledged for the financial support (No. 11052675) they provided for this project.*

REFERENCES

1. A.S. Warren, Developments and challenges for Aluminum – a Boeing perspective, *Materials Forum*., **28**, 24 (2004).
2. T. Dursun, C. Soutis, Recent developments in advanced aircraft aluminium alloys, *Materials and Design*., **56**, 862 (2014).
3. F. Snogan, C. Blanc, G. Mankowski, N. Pébère, Characterisation of sealed anodic films on 7050 T74 and 2214 T6 aluminium alloys, *Surf. Coat. Technol*., **154**, 94 (2002).
4. M.C. Vasco, A.N. Chamos, Sp.G. Pantelakis, Effect of environment's aggressiveness on the corrosion damage evolution and mechanical behavior of AA 2024-T3, *Fatigue and Fracture of Engineering Materials and Structures*., **40**, 1551 (2017).
5. M.L. Zheludkevich, R. Serra, MF. Montemor, I.M. Miranda Salvado, M.G.S. Ferreira, Corrosion protective properties of nanostructured sol–gel hybrid coatings to AA2024-T3, *Surf. Coat. Technol*., **200**, 3084 (2006).
6. M.L. Zheludkevich, R. Serra, M.F. Montemor, K.A. Yasakau, I.M.M. Miranda Salvado, M.G.S. Ferreira, Nanostructured sol–gel coatings doped with cerium nitrate as pre-treatments for AA2024-T3: Corrosion protection performance, *Electrochimica Acta*., **51**, 208 (2005).
7. M. Schem, T. Schmidt, J. Gerwann, M. Wittmar, M. Veith, G.E. Thompson, I.S. Molchan, T. Hashimoto, P. Skeldon, A.R. Phani, S. Santucci, M.L. Zheludkevitch, CeO_2-filled sol–gel coatings for corrosion protection of AA2024-T3 aluminium alloy, *Corros. Sci.*, **51**, 2304 (2009).
8. N. Pirhady Tavandashti, S. Sanjabi, Corrosion study of hybrid sol–gel coatings containing boehmite nanoparticles loaded with cerium nitrate corrosion inhibitor, *Prog. Org. Coat.*, **69**, 384 (2010).
9. J.B. Cambon, J. Esteban, F. Ansart, J.P. Bonino, V. Turq, S.H. Santagneli, C.V. Santilli, S.H. Pulcinelli, Effect of cerium on structure modifications of a hybrid sol–gel coating, its mechanical properties and anti-corrosion behavior, *Mater. Res. Bull.*, **47**, 3170 (2012).
10. L.E. Morales Palomino, Z. Paszti, I. Vieira Aoki, H. Gomes de Melo, Comparative investigation of the adhesion of Ce conversion layers and silane layers to a AA 2024-T3 substrate through mechanical and electrochemical tests, *Materials Research*., **10**(4)., 399 (2007).
11. X. Yu, C. Cao, Electrochemical study of the corrosion behavior of Ce sealing of anodized 2024 aluminum alloy, *Thin Solid Films*, **423**, 252 (2003).
12. B. Priet, G. Odemer, C. Blanc, K. Giffard, L. Arurault, Effect of new sealing treatments on corrosion fatigue lifetime of anodized 2024 aluminium alloy, *Surface and Coatings Technology*, **307**, 206 (2016).
13. O. Van der Biest, L.J. Vandeperre, Electrophoretic Deposition of Materials, *Annu. Rev. Mater. Sci.,* **29**, 327 (1999).
14. L. Besra, M. Liu, A review on fundamentals and applications of electrophoretic deposition (EPD), *Prog. Mater. Sci*., **52**, 1 (2007).
15. E. Antonelli, R. Santos da Silva, Electrophoretic deposition of $BaTi_{0.85}Zr_{0.15}O_3$ nanopowders, *Materials Research*, **16**(6), 1344 (2013).
16. R. Dula Corpuz, J. Rayala Albia, Electrophoresis fabrication of ZnO/ZnO-CuO composite for ammonia gas sensing, *Materials Research,* **17**(4), 851 (2014).
17. B. Fori, P.L. Taberna, L. Arurault, J.P. Bonino, C. Gazeau, P. Bares, Electrophoretic impregnation of porous anodic aluminum oxide film by silica nanoparticles, *Colloids Surf.A: Physicochem. Eng. Asp.*, **415**, 187 (2012).
18. B. Fori, P.L. Taberna, L. Arurault, J.P. Bonino, Decisive influence of colloidal suspension conductivity during electrophoretic impregnation of porous anodic film supported on 1050 aluminium substrate, *J. Colloid Interface Sci.*, **413**, 31 (2014).
19. K. Kusdianto, M. Nazli Naim, K. Sasaki, I. Wuled Lenggoro, Immobilization of colloidal particles into sub-100 nm porous structures by electrophoretic methods in aqueous media, *Colloids Surf. A: Physicochem. Eng. Asp.*, **459**, 142 (2014).

20. J. Escobar, L. Arurault, V. Turq, Improvement of the tribological behavior of PTFE-anodic film composites prepared on 1050 aluminum substrate, *Appl. Surf. Sci.*, **258**, 8199 (2012).
21. F. Caubert, P.L. Taberna, L. Arurault, Innovating pulsed electrophoretic deposition of boehmite nanoparticles dispersed in an aqueous solution, into a model porous anodic film, prepared on aluminium alloy 1050, *Surface and Coatings Technology*, **302**, 293 (2016).
22. G.D. Davis, T.S. Sun, J.S. Ahearn, J.D. Venables, Application of surface behaviour diagrams to the study of hydration of phosphoric acid-anodized aluminium, *J. Mater. Sci*., **17**, 1807 (1982).
23. B.E. Yoldas, Alumina gels that form porous transparent Al_2O_3, *J. Mater. Sci.*, **10**, 1856 (1975).
24. J.P Dasquet, D. Caillard, E. Conforto, J.P. Bonino, R. Bes, Investigation of the anodic oxide layer on 1050 and 2024T3 aluminium alloys by electron microscopy and electrochemical impedance spectroscopy, *Thin Solid Films*, 371, 183 (2000).
25. I. Pires, L. Quintino, R.M. Miranda, Performance of 2024-T3 Aluminium Adhesive Bonded Joints, *Mater. Manuf. Process*., **20**, 175 (2005).
26. G. Zamora, L. Arurault, P. Winterton, R. Bes, Impact of the type of anodic film formed and deposition time on the characteristics of porous anodic aluminum oxide films containing Ni metal, *Chem. Pap.*, **65**(4), 460 (2011).
27. J.W. Diggle, T.C. Downie, C.W. Goulding, Anodic oxide films on aluminum, *Chem. Rev*., **69**, 365 (1969).
28. F. Le Coz, L. Arurault, S. Fontorbes, V. Vilar, L. Datas, P. Winterton, Chemical composition and structural changes of porous templates obtained by anodising aluminium in phosphoric acid electrolyte, *Surface and Interface Analysis*, **42**, 227 (2010).
29. F. Le Coz, L. Arurault, L. Datas, Chemical analysis of a single basic cell of porous anodic aluminium oxide templates, *Materials Characterization*, **61**, 283 (2010).